Available online at www.sciencedirect.com
ScienceDirect
Trans. Nonferrous Met. Soc. China 21(2011) 2037−2043
Transactions of Nonferrous Metals Society of China
www.tnmsc.cn

Structure and properties of nanostructured Cu-13.2Al-5.1Ni shape memory alloy produced by melt spinning

M. IZADINIA, K. DEHGHANI

Department of Mining and Metallurgical Engineering, Amirkabir University of Technology, Tehran, Iran

Received 23 September 2010; accepted 5 January 2011

Abstract: The microstructure and properties of nanostructured Cu-13.2Al-5.1Ni shape memory alloy (SMA) were compared with those of initial coarse structure. The nanostructured Cu-Al-Ni ribbons were produced via rapid solidification using melt spinning technique. The structure and properties of both nanostructured and coarse-grain specimens were then characterized using XRD, SEM, AFM and DSC techniques. According to the obtained results, the nanostructured ribbons show one way shape memory effect. Besides, the formation of nanoparticles of γ_2 (Cu_9Al_4) and the nanograins results in a significant decrease in the martensite↔austenite transformation temperature. The produced nanostructure not only leads to a considerable increase in the recovered deformation but also results in the structure stability when it is subjected to deformation-recovery cycles.

Key words: Cu-Al-Ni shape memory alloys; melt spinning; rapid solidification; nanostructure

1 Introduction

The shape memory alloys such as Cu-based binary and ternary (Cu-Zn, Cu-Al, Cu-Zn-Al and Cu-Al-Ni) and Ni-Ti are usually used as functional actuators and sensors [1]. Compared these two groups, the Cu-based shape memory alloys (SMAs) exhibit inferior mechanical properties and lower shape memory effect attributed mostly to the coarse grains of Cu-based SMAs [2−3]. Thus, by modifying the microstructure, the aforementioned properties of the Cu-based SMAs can be improved. Regarding the grain refinement, one practical approach is using rapid solidification technique [4]. On the other hand, from the industrial point of view, the Cu-based SMAs are much more economical than Ni-Ti alloys due to their lower manufacturing costs as well as their easy production.

One practical way to significantly modify the structure is rapid solidification method. Among the rapid solidification techniques, melt spinning is a well known approach exhibiting unique advantages in refining the microstructure [5]. During melt spinning, a very high cooling rate of 10^5−10^7 K/s can be achieved readily [6]. In such a case, the solidification can take place in milliseconds. DEHGHANI et al [7−8] reported that the nanostructures produced by melt spinning exhibited a significant improvement in homogeneity and segregation, the appearance of metastable phases, a considerable fine dispersion of secondary phase, and an increase in the solid solubility.

The aim of the present work was therefore to study the effect of nanostructured Cu-13.2%Al-5.1%Ni on its shape memory effects. Besides, the structure and properties of both nanostructure and coarse-grain specimens were characterized and compared using X-ray diffraction (XRD), scanning electron microscopy (SEM) and atomic force microscopy (AFM) techniques.

2 Experimental

The material used in the present study was Cu-13.2%Al-5.1%Ni shape memory alloy. The alloy was prepared using a high-frequency induction furnace under argon atmosphere. Then, the samples of 60 mm×30 mm×0.9 mm were prepared from the cast ingot. The specimens were then solution treated at 950 °C (i.e. in β-phase region) for 1 h followed by water quenching to obtain an ordered metastable β phase.

The melt-spun ribbons were produced by injecting the melt onto a rotating copper wheel of 280 mm in diameter. The wheel speed was set at its highest amount,

Corresponding author: K. DEHGHANI; Tel: +98-21-64542900; Fax: +98-21-66405846; E-mail: dehghani@aut.ac.ir

DOI: 10.1016/S1003-6326(11)60969-2

around 40 m/s, to apply the highest cooling rate possible which was about 10^7 K/s. The thickness of produced ribbon was about 20 μm. The melt-spinning process is schematically shown in Fig. 1.

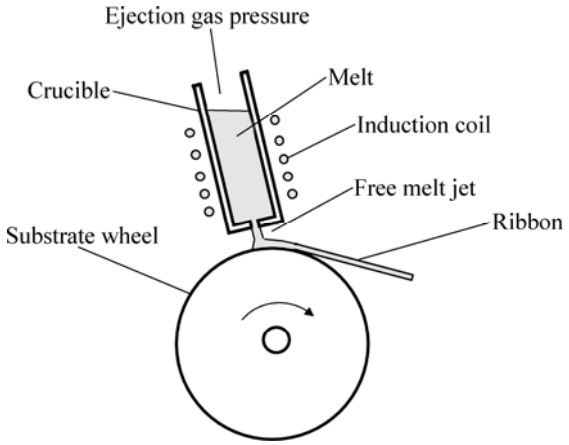

Fig. 1 Schematic of melt spinning process

The melt-spun specimens were etched using a solution consisted of 96 mL methanol, 2 mL HF and 2 g $FeCl_3$. The nanostructure ribbons were then characterized using a Philips-XL30 scanning electron microscope equipped with an energy-dispersive X-ray analyzer. The XRD patterns were also used to identify the formed phases. The XRD measurements were carried out in an X-Pert-Pro 2001 diffractometer using Cu K_α radiation operated at 40 kV and 20 mA. The transformation temperature of martensite↔austenite regarding the coarse grain and nanostructured samples was determined by differential scanning calorimetry (DSC) technique. The DSC measurements were carried out at the temperature range of 50−250 °C using Q100 model thermal analyzer. The employed heating and cooling rate was 10 °C/min.

To compare the shape memory effect of nanostructured ribbons and coarse grain samples, they were bent 90° around a cylinder having a diameter of D (Fig. 2). To measure their recovery, as a criterion for shape memory effect, the bent specimens were heated to 250 °C in an oil bath.

The applied deformation or strain (ε) and the recovered shape memory (η) were calculated as follows [9−11]:

$$\varepsilon=\left(\frac{t}{D+t}\right)\times 100\% \quad (1)$$

$$\eta=\left(\frac{90-\theta}{90}\right)\times 100\% \quad (2)$$

where θ is the residual angle, t is the specimen thickness and D is the diameter of cylinder used for bending test.

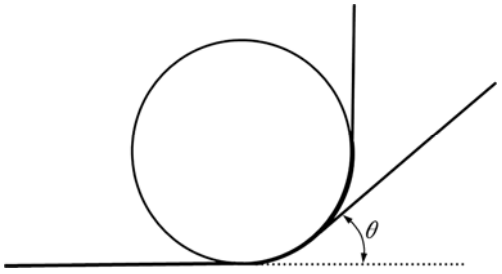

Fig. 2 Arrangement of shape memory effect measurement

3 Results and discussion

3.1 Microstructure

Figures 3(a)−(d) illustrate respectively the X-ray diffraction (XRD) patterns taken from the as-cast coarse structure, solution treated specimen (soaking at 950 °C for 1 h followed by water quenching), wheel side as well as the free side of melt-spun ribbons.

Considering Fig. 3(a), the XRD result confirms the presence of γ_2 (Cu_9Al_4) compound and α (Cu-Al-Ni) solid solution. This indicates that β phase undergoes the

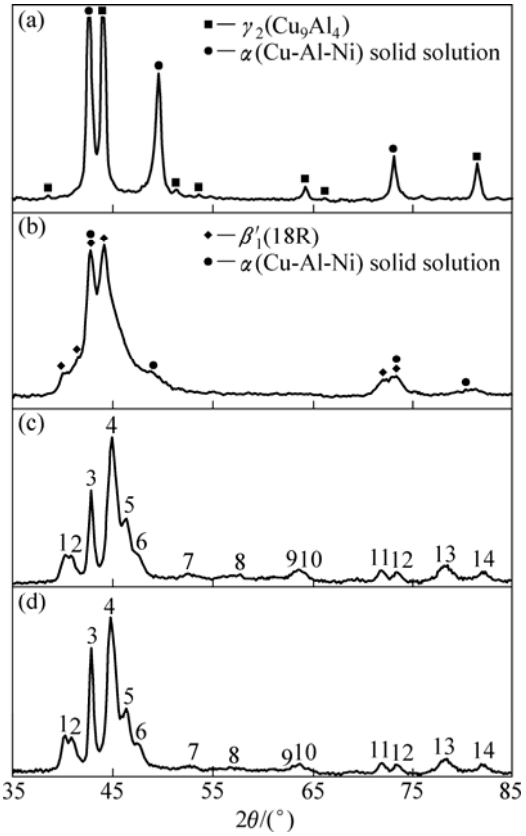

Fig. 3 XRD patterns of as-cast sample (a), solution treated at 950 °C for 1 h and water quenched (b), wheel-side (c) and free-side of melt-spun (d): 1—$\beta'_1(11\ \bar{2}\ )$; 2—$\beta'_1(202)$; 3—$\beta'_1(0018)$, $\beta_1(220)$; 4—$\beta'_1(12\ \bar{8}\ )$; 5—$\beta'_1(208)$; 6—$\beta'_1(20\ \bar{1}\ 0\ )$; 7—$\beta_1(222)$; 8—$\beta'_1(20\ \bar{1}\ \bar{6}\ )$; 9—$\beta'_1(12\ \bar{2}\ 0\ )$; 10—$\beta_1(400)$; 11—$\beta'_1(040)$; 12—$\beta'_1(320)$; 13—$\beta'_1(12\ \bar{2}\ \bar{6}\ )$; 14—$\beta'_1(32\ \bar{1}\ \bar{2}\ )$, $\beta_1(422)$

eutectoid decomposition of $\beta \rightarrow \alpha+\gamma_2$ due to slow cooling rate. Figure 3(b) shows the XRD pattern of the sample solution treated at 950 °C for 1 h followed by water quenching. Obviously, the matrix consists of α and β'_1 martensite that has the monoclinic 18R structure. Figures 3(c) and (d) present the X-ray diffraction patterns taken from the both sides of the nanostructured samples. In this case, the phases present in the structure are identified as β_1 and β'_1 that are in consistent with the results reported by other researchers [12]. The low intensity of the β_1 peaks indicates that there is some untransformed austenite phase. No peak related to the intermetallic phase of Cu, Al and Ni was observed. However, the absence of peaks concerning the intermetallic phases may not point out to the lack of these phases. This is because the detection limit by X-ray diffraction technique is typically about 5% (volume fraction) [13]. Thus, the absence of the intermetallic peaks implies the extended solid solubility of elements such as Al and Ni in the matrix.

The size of grains formed in melt-spun ribbons was determined using the following equation [14]:

$$d = \frac{K\lambda}{\beta \cos\theta} \tag{3}$$

where K is a constant that depends on the crystallite shape and is about 0.89; λ is the wavelength (Cu K_α radiation); β is the full width at half max (FWHM) and θ is the Bragg angle. Using Eq. (3), the grain size (d) was determined to be about 72 nm for wheel side and 124 nm for free side of melt-spun ribbons.

Figures 4(a) and (b) present respectively the optical microstructures of conventional as-cast sample and solution treated specimen followed by water quenching.

As obvious, the initial coarse structure is quite different from that produced by solution treated followed by water quenching. In case of as-cast structure (Fig. 4(a)), the particles distributed in α matrix are mostly intermetallic γ_2 phase. There is no sign of martensite plate in the as-cast structure. However, in case of solution treated specimen (Fig. 4(b)), the martensite plates, identified as β'_1 [15], exhibit different orientations in different grains. For example, the V-shape martensite is formed in some regions, while in other areas within the matrix, needlelike martensite can be observed, as shown in Fig. 4(b).

Figure 5 shows the morphological images of the melt-spun Cu-Al-Ni ribbon.

The optical micrograph taken from the thickness of the melt-spun ribbon is presented in Fig. 5(a); whereas, the cross-sectional microstructure of nanostructured ribbons is observed in Fig. 5(b). In general, two distinct structures can be recognized: a featureless structure formed on the chilled side of the ribbons, and a columnar

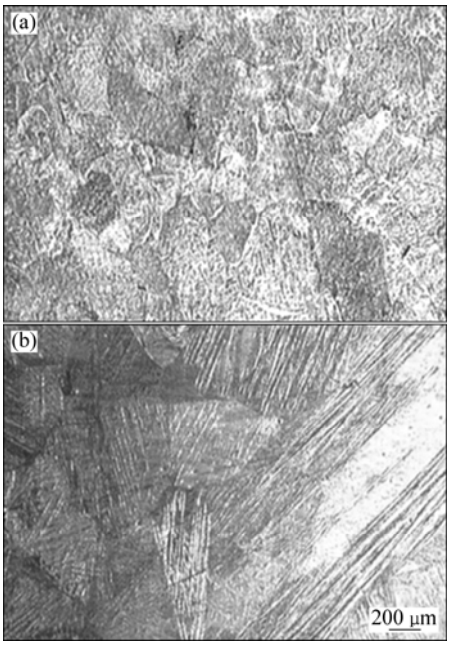

Fig. 4 Optical micrographs of Cu-13.2%Al-5.1%Ni: (a) As-cast sample; (b) Solution treated at 950 °C for 1 h and then water quenched

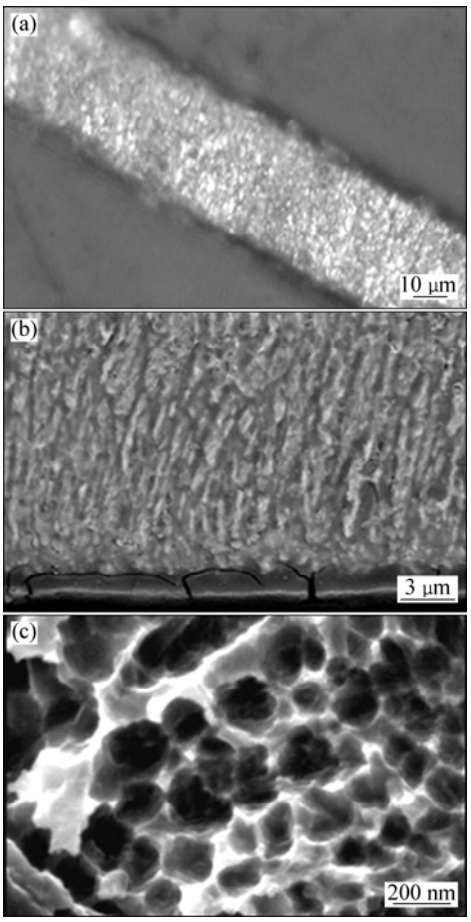

Fig. 5 Morphological images of as-spun Cu-Al-Ni ribbon: (a) Optical micrograph of ribbon; (b) SEM image of transverse section of melt-spun ribbon; (c) SEM image of nanograin formed in melt-spun ribbon

one regarding the free side of specimen. The featureless zone is a unique region formed due to rapid solidification of present alloy. The featureless term is used because of significant grain refining, leading to the formation of nanograins in this zone. Thus, the nanograins are formed as a result of rapid solidification at very high cooling rate of about 10^7 K/s [7−8, 16]. The columnar zone consists of columnar grains oriented vertically to the wheel surface and in the direction of heat flow. The coarse grains are not observed in the melt-spun ribbons. The absence of equiaxed region can be somehow attributed to the absence of both second phase particles at the grain boundaries [17] and solute pile-up ahead of solidification interface. The latter causes constitutional super cooling. The SEM image of nanograins formed in melt-spun specimen is illustrated in Fig. 5(c).

In another approach, the nanostructure of the as-spun Cu-Al-Ni ribbon was also investigated by AFM technique to confirm the formation of nanograins. The AFM images taken from the produced Cu-Al-Ni ribbon are observed in Fig. 6. These micrographs confirm clearly the formation of nanosized grains.

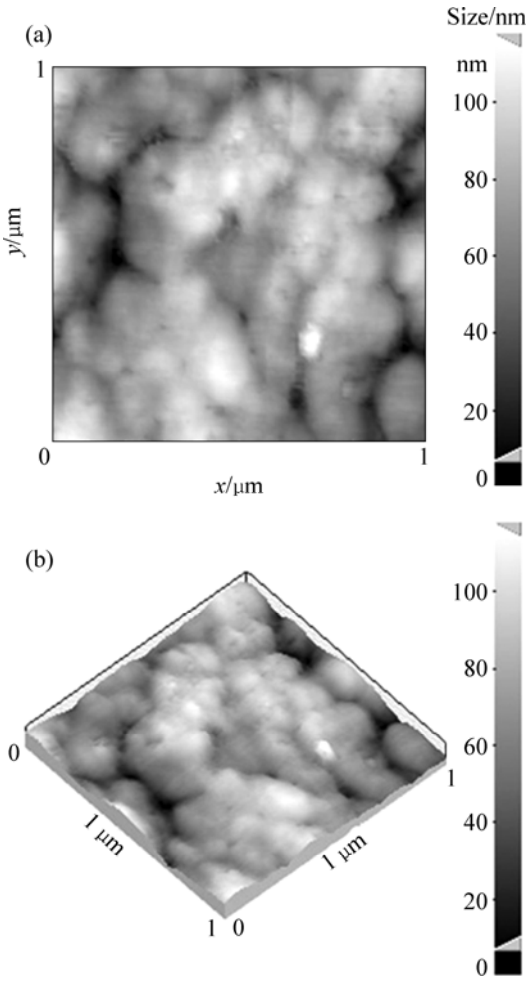

Fig. 6 AFM micrographs confirming formation of nanograins in melt-spun ribbon: (a) 2D topography; (b) 3D topography

The microstructures of conventional as-cast specimen and melt-spun ribbons are compared in Fig. 7. In case of melt-spun structure, there are some nanoprecipitates. Figure 8 illustrates the EDX pattern taken from the nanoprecipitates. The EDX results confirm the presence of nanoparticle γ_2 (Cu_9Al_4) formed during the melt spinning process. According to the EDX results, although the nanoparticles are rich in Ni (containing about 4.9% Ni) but their Ni content is still lower than that of matrix with 5.1% Ni. According to Fig. 7(b), nanoparticles are very fine dispersed within the matrix having an inter-particle spacing of about 300 nm. By contrast, in case of coarse structure, the γ_2 particles exhibit a coarse dispersion with the average size of 0.8 μm (Fig. 7(a)).

A major concern regarding the nanostructured

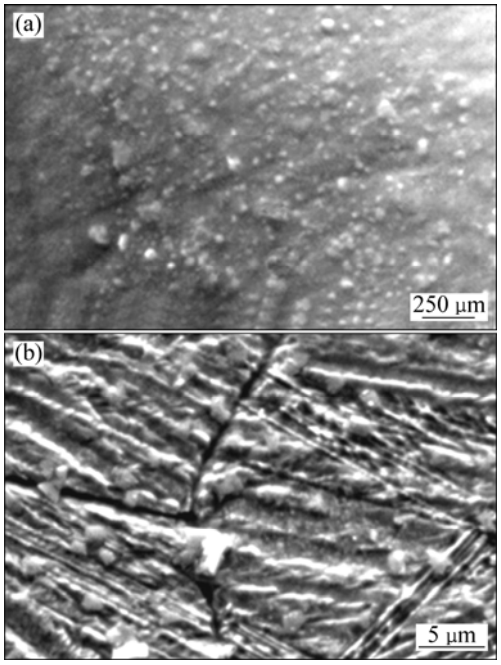

Fig. 7 SEM micrographs of γ_2 precipitates: (a) Conventional structure indicating microsize γ_2 precipitates; (b) Melt-spun structure indicating nanosize γ_2 precipitates

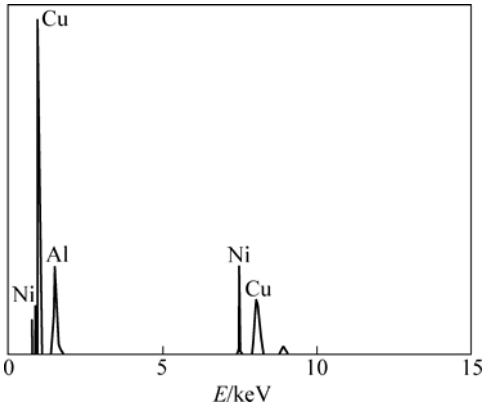

Fig. 8 EDX pattern of melt-spun foils indicating nanosize γ_2 precipitates

materials is their thermal instability. That is because there is a large driving force for grain growth due to the high volume fraction of grain boundaries, especially at elevated temperatures. The instability of nanograin materials, which leads to the grain growth, is deleterious to the mechanical properties of these materials. However, a very fine dispersion of nanosized particles can significantly prevent the grain-boundary mobility by exerting a pinning force on the grain boundaries, as reported by DEHGHANI et al [7−8]. This phenomenon is known as Zener pinning. In the present work and in case of nanostructured specimens, the Zener pinning raised from the nanoparticles can exert a strong force on the grain boundaries to prevent their growth/mobility. The formation of nanosized γ_2 (average size of 25 nm) can significantly pin the grain boundaries to inhibit their motion. By contrast, in case of the specimen solution treated at 950 °C for 1 h followed by water quenching, the particles are too coarse (0.8−1.0 μm) to exert Zener drag.

3.2 Transformation temperature

The transformation characteristics of initial and melt-spun samples are evaluated using DSC technique. Figure 9 compares the DSC results (on heating and cooling) of the solution-treated and melt-spun specimens. In both cases, an exothermic peak during the cooling (martensitic transformation) and an endothermic peak during the heating (reverse martensitic transformation) are observed. However, the characteristics of DSC curves indicate that the transformation temperatures in case of nanostructured samples are shifted towards lower temperatures comparing with the coarse one. Besides, the peaks become smaller and wider in case of nanostructured specimens.

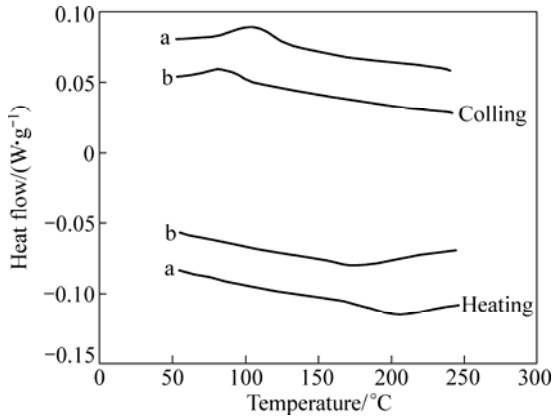

Fig. 9 DSC curves of conventional structure (a) and nanostructured samples (b)

The transformation temperatures regarding the nanostructure specimens and those of initial structures are summarized in Table 1. Referring to Fig. 9, the following mechanisms can be responsible for the differences in the DSC results of both cases.

Table 1 Transformation temperature (°C) characteristics of melt-spun ribbons and conventional sample

Cu-13.2%Al-5.1%Ni	A_s	A_f	M_s	M_f
Ingot	166	218	131	70
Melt-spun	157	185	104	55

1) The rapid solidification due to the high cooling rate can produce extensive dislocation densities which can in turn provide numerous heterogeneous nucleation sites for martensite formation.

2) Considering the dependence of martensite formation on internal stress [18], it is expected that the significant internal stresses in case of nanostructured case [19] will enhance the formation of martensite phase.

3) Grain size is another important factor that can significantly affect the martensite transformation. In general, for the materials experiencing martensite transformation, the ones with finer grains can result in smaller martensite-plate size [18]. Besides, as the grain size of parent phase decreases, the martensite transformation can be fully or partially suppressed [20]. This is justified by inverse relation between the shear strength of parent phase and grain size.

4) Applying a high cooling rate results in a great vacancy concentration which in turn enhances the ordering transformation. An order structure exhibits more sharing strength, consequently, it offers more resistance to martensitic transformation. It is reported that ordering process, occurred due to high cooling, can result in a decrease in martensite transformation temperature [21].

Therefore, all the aforementioned mechanisms can somehow contribute to the behavior illustrated in Fig. 9 though the decrease in transformation temperature implies that grain size and ordering process can have more contribution in this regard. This is in consistent with the work of FONT et al [22] who found a decrease in the transformation temperature after the rapid solidification by melt spinning.

3.3 Shape memory effect

The shape memory effects of solution-treated sample and melt-spun one were measured using Eqs. (1) and (2). The results are compared in Fig. 10. These samples were strained to 1%, 3% and 5% followed by recovering at 250 °C. It is of significant importance that, in case of nanostructured samples, the recovery of shape memory is about 100% and it remains at this level even after 100 deformation-recovery cycles. In case of solution- treated (soaking at 950 °C for 1 h followed by water- quenching) samples, the shape memory recoveries

are 58%, 44%, and 28% after 1%, 3%, and 5% deformation, respectively.

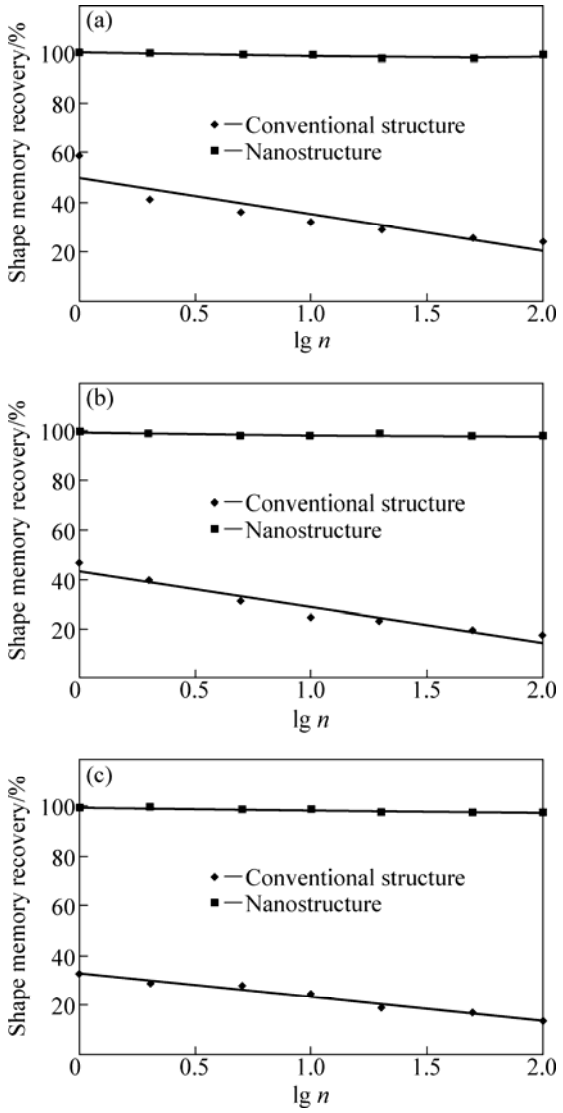

Fig. 10 Shape memory recovery of nanostructured and conventional structures as a function of bending and heating cycles: (a) Deformation strain 1%; (b) Deformation strain 3%; (c) Deformation strain 5%

The much smaller recoveries in case of coarse samples can be attributed to the occurrence of intergranular fracture because of its coarse grain. The occurrence of intergranular fracture is pronounced not only by coarse grains but also by grain boundary segregation [23]. Comparing with the past works, although there are some works on producing the CuAlNi alloy by melt spinning [4, 22, 24], none of them reported the formation of nanostructured Cu-based shape memory alloy. Besides, in some cases, the researchers performed an additional treatment to enhance the shape memory effect of this alloy. For example, LOVEY et al [25] reported that they conducted an additional heat treatment to enhance shape memory effect of CuAlNi alloy. However, the applied treatment resulted in extensive grain growth.

According to the obtained results, not only the nanostructured Cu based shape memory alloy was produced by melt spinning, but also significant increase in shape memory effect was observed comparing with the coarse structure of this alloy. Besides, the pronounced nanostructure exhibits significant structure homogeneity due to rapid solidification.

4 Conclusions

1) The structure and properties of nanostructured Cu-Al-Ni shape memory alloy (SMA) are compared with the coarse structure of this alloy. The nanostructured Cu-Al-Ni SMA exhibits unique properties comparing with its initial cast structure.

2) The nanostructure obtained by melt spinning technique results in remarkable enhancement of shape memory properties in comparison to coarse-grain structure. That is because the nanoparticles and nanograins produced by melt spinning exhibit significant effects on the properties and the structure stability of nanostructure Cu-Al-Ni SMA. Besides, the produced nanostructure can lead to excellent structure homogeneity.

References

[1] NIKOLAEV V I, PULNEV S A, MALYGIN G A, SHPEIZMAN V V, NIKANOROV S P. Pseudoelastic deformation and generation of reactive stresses in a Cu-Al-Ni shape memory alloy in the temperature range 4.2−293 K [J]. Physics of the Solid State, 2007, 49: 1878−1883.

[2] OTSUKA K, SAKAMOTO H, SHIMIZU K. Successive stress-induced martensitic transformations and associated transformation pseudoelasticity in Cu-A1-Ni alloys [J]. Acta Metallurgica, 1979, 27: 585−601.

[3] SUGIMOTO K, KAMEI K, MATSUMOTO H, KOMATSU S, AKAMATSU K, SUGIMOTO T. Grain-refinement and the related phenomena in quaternary Cu-Al-Ni-Ti shape memory alloys [J]. Journal de Physique, 1982, 43: 761−766.

[4] LOJEN G, ANZEL I, KNEISSL A, KRIZMAN A, UNTERWEGER E, KOSEC B, BIZJAK M. Microstructure of rapidly solidified Cu-Al-Ni shape memory alloy ribbons [J]. Journal of Materials Processing Technology, 2005, 162−163: 220−229.

[5] LIBERMANN HOWARD H. Rapidly solidified alloys: Processes, structures, properties, applications materials [M]. New York: CRC Press, 1993: 254.

[6] ANANTHARMAN T R, SURYANARAYANA C. Rapidly solidified metals [M]. Switzerland: Tans Tech Publisher, 1987: 5.

[7] DEHGHANI K, MARYAM S, MINA S, ABOUTALEBI H. Comparing the melt-spun nanostructured aluminum 6061 foils with conventional direct chill ingot [J]. Mater Sci Eng A, 2008, 489: 245−252.

[8] SALEHI M, DEHGHANI K. Structure and properties of nanostructured aluminum A413.1 produced by melt spinning compared with ingot microstructure [J]. J Alloys Compd, 2008, 457: 357−361.

[9] TANG S M, CHHUNG C Y, LIU W G. NiTiCu shape memory alloy produced by powder technology [J]. J Mater Process Technol, 1997, 63: 307−312.
[10] XIAO Zhu, LI Zhou, FANG Mei, XIONG Shi-yun, SHENG Xiao-fei, ZHOU Meng-qi. Effect of processing of mechanical alloying and powder metallurgy on microstructure and properties of Cu-Al-Ni-Mn alloy [J]. Materials Science and Engineering A, 2008, 488: 266−272.
[11] LI Z, PAN Z Y, TANG N, JIANG Y B, LIU N, FANG M, ZHENG F. Cu-Al-Ni-Mn shape memory alloy processed by mechanical alloying and powder metallurgy [J]. Materials Science and Engineering A, 2006, 417: 225−229.
[12] SABURI T, WAYMAN C M. Crystallographic similarities in shape memory martensites [J]. Acta Metall, 1979, 27: 979−995.
[13] ÜNLÜ N, GENÇ A, OVECOGLU M L, ERUSLU N, FROES F H. Characterization investigations of melt-spun ternary Al-*x*Si-3.3Fe (*x*=10, 20wt.%) alloys [J]. J Alloys Compd, 2001, 322: 249−256.
[14] CULLITY B D. Elements of X-ray diffraction [M]. Vol. 1, 2nd ed. Massachusetts: Addison-Wesley Pub Co, 1978: 87.
[15] PICORNELL C, PONS J, CESARI E. Effects of thermal aging in *β*-phase in Cu-Al-Ni single crystals [J]. Physique IV, 1997, 7: 323−331.
[16] SATER J M, SANDERS T H, GARRETT R K. Characterization of rapidly solidified materials [M]//FINE M E, STARKE E A. Rapidly Solidified Powder Aluminium Alloys Symposium. 1984: 83−117.
[17] van ROOYEN M, van der PER N M, KATGERMAN L, de KEIJSER T H, MITTEMEIJER E J. Rapidly quenched metals [M]. Amsterdam, The Netherlands: Elsevier Science Publishers, 1985: 823-826..
[18] PORTER D A, ESTERLING K E. Phase transformation in metals and alloys [M]. 2nd ed. London: Chapman Publication and Hall, 1992: 235.
[19] YAZDIPOUR A, SHAFEI M A, DEHGHANI K. Modeling the microstructural evolution and effect of cooling rate on the nanograins formed during the friction stir processing of Al5083 [J]. Materials Science and Engineering A, 2009, 527: 192−197.
[20] GLEZER A M, BLINOVA1 E N, POZDNYAKOV V A, SHELYAKOV A V. Martensite transformation in nanoparticles and nanomaterials [J]. Journal of Nanoparticle Research, 2003, 5: 551−560.
[21] OTSUKA K, REN X. Factors affecting the M_s temperature and its control in shape memory alloys [J]. Mater Sci Forum, 2002, 394−395: 177−184.
[22] FONT J, CESARI E, MUNTASELL J, PONS J. Thermomechanical cycling in Cu-Al-Ni-based melt-spun shape memory ribbons [J]. Materials Science and Engineering A, 2003, 354: 207−211.
[23] AMELINCKX S, DEKEYSER W. The structure and properties of grain boundaries [J]. Solid State Phys, 1959, 8: 325−499.
[24] MALARR´IA J, ELGOYHEN C, VERMAUT P H, OCHIN P, PORTIER R. Shape memory properties of Cu-based thin tapes obtained by rapid solidification methods [J]. Materials Science and Engineering A, 2006, 438−440: 763−767.
[25] LOVEY F C, CONDO A M, GUIMPEL J, YACAMAN M J. Shape memory effect in thin films of a Cu-Al-Ni alloy [J]. Materials Science and Engineering A, 2008, 481−482: 426−430.

熔体旋淬法制备纳米 Cu-13.2Al-5.1Ni 形状记忆合金的结构和性能

M. IZADINIA, K. DEHGHANI, H. MOHAMADI

Department of Mining and Metallurgical Engineering, Amirkabir University of Technology, Tehran, Iran

摘　要：比较了纳米 Cu-13.2Al-5.1Ni 形状记忆合金和初始粗晶结构合金的结构和性能。采用熔体旋淬技术，通过快速凝固制备纳米 Cu-Al-Ni 薄带。利用 XRD、SEM、AFM 和 DSC 等技术表征了纳米结构和粗晶样品结构及性能。结果表明，纳米结构薄带显示了单次形状记忆效应。另外，生成的纳米 $\gamma_2(Cu_9Al_4)$粒子和纳米晶粒导致马氏体↔奥氏体相变温度显著降低。经过变形−回复循环后，所制备的纳米结构不仅导致回复变形量大幅增加，而且导致结构稳定性增加。

关键词：Cu-Al-Ni 形状记忆合金；熔体旋淬；快速凝固；纳米结构

(Edited by LI Xiang-qun)